IEEE Access
Multidisciplinary | Rapid Review | Open Access Journal

Received July 2, 2019, accepted July 22, 2019, date of publication July 26, 2019, date of current version August 13, 2019.

Digital Object Identifier 10.1109/ACCESS.2019.2931470

Cubature Information Gaussian Mixture Probability Hypothesis Density Approach for Multi Extended Target Tracking

ZHE LIU[1], LINNA JI[1], FENGBAO YANG[1], XIQIANG QU[1], ZHILIANG YANG[1], AND DONGZE QIN[2]

[1]School of Information and Communication Engineering, North University of China, Taiyuan 030051, China
[2]School of Mechatronics Engineering, North University of China, Taiyuan 030051, China

Corresponding author: Xiqiang Qu (quxiqiang@nuc.edu.cn)

This work was supported in part by the National Natural Science Foundation of China Projects under Grant 61702465, and in part by the Key Laboratory Open Research Fund Projects of Advanced Manufacturing Technology Laboratory, Shanxi, under Grant XJZZ201704.

ABSTRACT In multi-extended target tracking, each target may generate more than one observation. The traditional probability hypothesis density (PHD)-based methods are no longer effective in such scenarios. Recently, the Gaussian mixture PHD approach for the extended target tracking (ET-GM-PHD) has been presented to solve such a problem. The tracking performance of this approach has been restricted by the following disadvantages. First, it only focuses on the linear models. When targets are moving with nonlinear models, it may lead to great tracking errors. Second, the birth intensities are commonly assumed as a prior. In practice, these intensities are always unknown. In order to improve the tracking performance of the traditional ET-GM-PHD approach, a novel extended target tracking approach, namely the ET-cubature information GM-PHD (ET-CIGM-PHD) approach, has been proposed in this paper. To be more specific, we, first, utilize the cubature information filter (CIF) and gating methods to predict and update the Gaussian mixture components of the ET-GM-PHD approach. In the merit of high estimating accuracy of the CIF method, the tracking accuracy of the traditional ET-GM-PHD approach can be significantly improved. Due to the gating method, only part of cells can be used to construct the observation set in the update stage. Thus, the computational load of our approach can be significantly reduced. Then, we propose an adaptive initiating method for the birth intensity initiating. In our method, we utilize the estimated target set to select the most possible partition. Then, we remove cells associated with the estimated targets from the selected partition. The left cells are used to initiate the birth intensity. With the help of the above implementations, the birth intensity can be adaptively initiated. Using such a method, our approach can solve the cases that the prior information of birth intensity is rather little. The simulation results demonstrate the effectiveness of our approach.

INDEX TERMS Multi extended targets, Gaussian mixture, probability hypothesis density, cubature information filter.

I. INTRODUCTION

A. BACKGROUND

In multi-target tracking area, targets are commonly assumed to follow the standard target models. That is to say, each target can generate at most one observation (see Fig 1). However, for modern radars with high resolutions, targets may occupy several resolution cells. In these cases, each target may give rise to more than one observations (see Fig 2). Such targets are named as the extended targets [1]. Compared with the standard targets models, the observation models of extended targets require the following two components; the model for the number of observations generated by each target, and the model for spatial distribution of these observations [2]. Otherwise, the associations between observations are always unknown. Thus, the tracking approaches for multi targets, such as the nearest-neighbour Kalman filter (NNKF) [3], multiple hypothesis tracking (MHT) [4], and joint

The associate editor coordinating the review of this manuscript and approving it for publication was Weimin Huang.

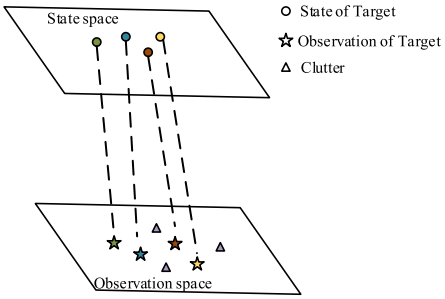

FIGURE 1. Standard target tracking. The state of the target have no more than one corresponding observation in the observation space. Here, we use the same color to represent the state and its corresponding observation.

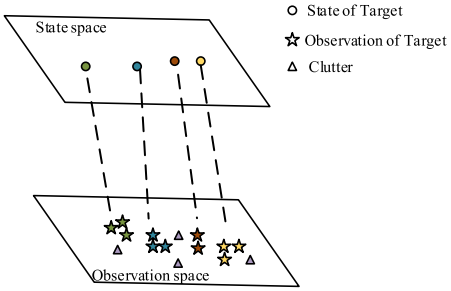

FIGURE 2. Extended target tracking. Each state may have more than one corresponding observations in the observation space. Here, we use the same color to represent the state and its corresponding observations.

probabilistic data association (JPDA) [5] can hardly be applied in the extended target tracking.

To solve the extended target tracking problem, several approaches have been presented. Using the random matrices, Feldmann and Franken [6]–[8] represented the target extension with a random symmetric positive definite matrix. Vivone *et al.* [9] applied the random matrix into multiple sensor scenarios. Magnant *et al.* [10] used the random matrix to track and classify extended targets in maritime surveillance. Although these approaches are efficient in ellipsoidal extended target tracking scenarios, it may give rise to inaccurate results in non-ellipsoidal extended target scenarios. Considering the non-ellipsoidal extended target as a combination of sub-ellipsoidal extended objects, Lan and Li [11] proposed a multiple-model (MM) approach to solve such a problem. In this approach, the sub-object motions are combined to model the dynamics of the non-ellipsoidal extended targets. On this basis, the MM method has been utilized to improve the estimating accuracy of the non-ellipsoidal extended target. However, the number of the sub-object is assumed as a prior. Beard *et.al.* [12] modeled the state of the extended target as a generalised labelled multi-Bernoulli (GLMB) component. Combined with the gamma Gaussian inverse Wishart (GGIW) distribution, a GLMB filter has been be developed for tracking the extended target. The improved versions of such an approach have been presented in [13] and [14]. These LMB based approaches can estimate the states and trajectories of the extended targets. Since the LMB approaches approximate the number of target after every update, it leads to a cumulative errors in the cardinality (the number of targets) distribution [14]. Moreover, their computation complexity is more expensive than the PHD based approaches. In the light of [15], Granström *et al.* [16] constructed the Poisson model for the extended target tracking. Pioneered by these literature, Mahler [1] formulated the observation-update equations of the probability hypothesis density (PHD) filter for the extended target tracking (called the EPHD). However, the EPHD filter is computationally intractable [17]–[20]. Granström *et al.* [21]–[23] proposed the Gaussian mixture implementation of the PHD filter for the extended target tracking (named as the ET-GM-PHD). The improved approach has been presented in [24]. The ET-GM-PHD approach utilizes the Gaussian mixture moments to represent the first-order moments, making the PHD filter of the extend targets tractable. Nevertheless, such an approach may lead to great tracking errors in nonlinear scenarios. Chen *et al.* [25] utilized the cubature Kalman filter into the ET-GM-PHD approach. It can improve the tracking accuracy in nonlinear scenarios. Since it simply uses all of the partitions to update intensities, the proposed approach may cost great computational complexity. In order to improve the tracking performance,Yang *et al.* [26] presented an improved ET-GM-PHD approach by introducing a penalty strategy into the likelihood computing. Zhang and Ji [27] proposed the ART partitioning method. By utilizing the fuzzy ART model into observation partitioning, the computational time can be decreased. Such a method has been used in [19]. However, the performance of this method dependents on the choice of the vigilance values. Shen *et al.* [28] proposed an extended target multipath tracking approach using multipath Bernoulli filter (MPBF) and ET-PHD filter. Nevertheless, it only uses one extended target. Ristic *et al.* [29] presented the birth initiating method for PHD and cardinalised PHD (CPHD). Zhu *et al.* [30] proposed a birth density estimating method. Zhou *et al.* [31] used the entropy distribution to remove the noise of the birth intensity. However, these methods are under the standard target assumption. Wu *et al.* [32] proposed an iterative random sample consensus (I-RANSAC) algorithm with a sliding window to initiate the birth intensity. In practice, selecting the width of the window is rather difficult. Peng and Ye [33] proposed the adaptive birth target initiation methods. However, these adaptive methods have two disadvantages. First, these methods utilize all of the partitions into birth intensity initiating. It may cost great computational time. Second, most of these methods assume that there is only one target born at each scan.

B. OUR WORK AND CONTRIBUTION

Currently, information filters such as EIF (extended information filter) and UIF (unscented information filter) are widely used in nonlinear target tracking. Compared with these filters, the cubature information filter (CIF) [34] method is easier in initiation, and more suitable to estimate states with the high dimension. Otherwise, it also has significant tracking performance in nonlinear target tracking. In the light

of [18], we integrate the CIF method and a gating method into the ET-GM-PHD approach in this paper. Here, we name our approach as the ET-cubature information GM-PHD (ET-CIGM-PHD) approach. Unlike the CIF and gating methods in standard target tracking, our approach aims at tracking multi extended targets in nonlinear scenarios. In such scenarios, the assumption of standard targets cannot be satisfied. Thus, the CIF and gating methods cannot be directly integrated into the ET-GM-PHD approach. To solve such a problem, first, we adopt the CIF method to predict and update the Gaussian mixture components of the ET-GM-PHD approach. Using such a method, the ET-GM-PHD approach can be extended into the nonlinear extended target tracking scenarios, and achieved high estimating accuracy. On this basis, we present a gating method to construct the observation set, and reduce the computational complexity of the CIF method. Then, to initialize the birth density of extended targets, inspired by [29],we propose an adaptive birth density initializing method for our approach. Using such a method, the birth density of our approach can be adaptively initialized. We list the main contributions as follows:

1) We propose an improved ET-GM-PHD approach based on the CIF and gating methods. First, we, following the way of the ET-GM-PHD approach, represent the density of the extended target by Gaussian mixture components. Then, we predict the states of Gaussian mixture components by the CIF method. In order to construct the observation set, and reduce the computational load of the CIF method, we propose a gating method to extract the cells corresponding to the current predicted observation. Then, these extracted cells are combined into one set (consists of observations). On this basis, we utilize the combined set to update the state and covariance of the CIF method. By iterating the CIF and gating methods, the states and covariances of the Gaussian mixture components can be obtained. With the obtained Gaussian mixture components, the intensities of multi extended target can be achieved. Unlike the traditional gating methods, we directly implemented our approach on cells, enjoying better computational complexity. Benefitted from these operations, the estimation accuracy and computational speed of our approach can be significantly improved.
2) We develop a birth intensity initiation method for our approach. In the multi extended target tracking, the estimated targets can be considered as the survival targets in current time step. That is to say, these targets may not be birth targets in next time step. According to this assumption, we remove the observations associated with the estimated targets. The left observations can be considered as the observations generated by the birth targets. To achieve this, we, first, project cells of each partition into state space. Then, we calculate the numbers of the projected cells associated with the estimated targets. The partition with largest number can be considered as the most possible partition. Thus, we can remove the cells associated with the estimated targets from such a partition. Since each cell may contain several observations, we define a contribution factor to combine each cell into one component. On this basis, the combined components are used to calculate the birth intensity. Therefore, the birth intensity can be adaptively initiated. Compared with the traditional adaptive method, our method can avoid the restrict of one target born at each scan, and enjoy less computational time.

The rest of this paper is organized as follows: we overview the PHD filter and GM-PHD implementation for extended targets in Section II. Section III proposes our ET-CIGM-PHD approach. Simulation results are demonstrated in Section IV, and Section V concludes this paper.

II. THE PHD FILTER AND GM-PHD FOR EXTENDED TARGET TRACKING

In this section, we, first, discuss the observation partitioning method of the multi extended targets in Section II-A. Then, the random finite set (RFS) and PHD functions are introduced in Section II-B. Section II-C and II-D overview the PHD filter of multi extended targets and ET-GM-PHD approach, respectively. The main notations are listed as follows:

$\mathbf{C}_i$	The i-th partition of the current observation set
$\mathbf{X}_k$	The state set of multi-target at time k
$\mathbf{Z}_k$	The observation set of multi-target at time k
$\mathbf{x}_k$	The state of a dynamic target at time k
$\mathbf{z}_k$	The observation of a dynamic target at time k
$N(\cdot)$	The function of the Gaussian distribution
$\gamma_k(\cdot)$	The birth intensity of target at time k
$p_s(\cdot)$	The survival probability of target
$p_d(\cdot)$	The detected probability of target
$D(\cdot\|\cdot)$	The intensity of multi-target

A. OBSERVATION PARTITIONING

In multi extended target tracking scenarios, each target may generate more than one observation. That means each target may generate a group of observations. Commonly, the associations between observations of different targets are always unknown. It poses a great challenge for observation partitioning. To illustrate such a challenge, let the observation set $\mathbf{Z}$ be $\mathbf{Z} = \{\mathbf{z}_1, \mathbf{z}_2, \mathbf{z}_3\}$, where $\mathbf{z}_i$ represents the i-th observation of $\mathbf{Z}$. All of the possible partitions can be listed as follows [1]:

$$\begin{aligned}
&\mathbf{C}_1 : \mathbf{W}_1^1 = \{\mathbf{z}_1, \mathbf{z}_2, \mathbf{z}_3\},\\
&\mathbf{C}_2 : \mathbf{W}_1^2 = \{\mathbf{z}_1\}, \quad \mathbf{W}_2^2 = \{\mathbf{z}_2, \mathbf{z}_3\},\\
&\mathbf{C}_3 : \mathbf{W}_1^3 = \{\mathbf{z}_1, \mathbf{z}_2\}, \quad \mathbf{W}_2^3 = \{\mathbf{z}_3\},\\
&\mathbf{C}_4 : \mathbf{W}_1^4 = \{\mathbf{z}_1, \mathbf{z}_3\}, \quad \mathbf{W}_2^4 = \{\mathbf{z}_2\},\\
&\mathbf{C}_5 : \mathbf{W}_1^5 = \{\mathbf{z}_1\}, \quad \mathbf{W}_2^5 = \{\mathbf{z}_2\}, \ \mathbf{W}_3^5 = \{\mathbf{z}_3\},
\end{aligned}$$

where $\mathbf{W}_j^i$ denotes the j-th cell of the partition $\mathbf{C}_i$.

Obviously, when the number of observations increases, the number of possible partitions grows even larger. It may make the PHD computing rather expensive. In [24],

Granstrom *et al.* presented a distance partition method to solve such a problem. It only utilizes the subset of partitions for the PHD computing, making better performance than the Kmeans clustering method. In this paper, we tend to use the distance partition method in [24].

B. RANDOM FINITE SET AND PHD FUNCTIONS

1) RANDOM FINITE SET OF MULTI TARGETS

In multi-target tracking scenario, the states and observations of targets belong to sets of the individual target states and observations, respectively. Since the targets appear, disappear, and maneuver, the target number and states are uncertain at different time. In addition, influenced by the imprecise detections, the observations of targets are also uncertain in the tracking process. Thus, the RFS is used to represent the multi-target states and observations.

Here, we assume that there are M_k targets in the multi-target tracking scenario at time k. The state vector of each target at time k is represented by $\mathbf{x}_{k,i}$, where i denotes the i-th target. Obviously, $\mathbf{x}_{k,i}$ is in the state space $\mathfrak{X}$. Assuming that the multi-target state set at time k is represented by $\mathbf{X}_k$, we have

$$\mathbf{X}_k = \{\mathbf{x}_{k,1}, \mathbf{x}_{k,2}, \ldots, \mathbf{x}_{k,M_k}\}. \tag{1}$$

Since $\mathbf{X}_k$ is constructed by several states of individual targets, we have $\mathbf{X}_k \in \mathcal{F}(\mathfrak{X})$, where $\mathcal{F}(\mathfrak{X})$ is the set of all finite subset in the state space $\mathfrak{X}$. Due to targets appearing, disappearing and maneuvering, $\mathbf{x}_{k,i}$ and the dimension (also called cardinality) of $\mathbf{X}_k$ are uncertain. In addition, the number of multi-target in tracking process is finite without ordering for the individual targets. Thus, $\mathbf{X}_k$ is a random finite set in $\mathcal{F}(\mathfrak{X})$.

Similarly, if there are N_k observations at time k, the multi-target observation set $\mathbf{Z}_k$ at time k can be modeled by

$$\mathbf{Z}_k = \{\mathbf{z}_{k,1}, \mathbf{z}_{k,2}, \cdots, \mathbf{z}_{k,N_k}\}, \tag{2}$$

where $\mathbf{z}_{k,j} \in \mathfrak{Z}$ is the j-th target observation vector at time k. Let $\mathcal{F}(\mathfrak{Z})$ be the set of all finite subset in the observation space $\mathfrak{Z}$. Therefore, we have $\mathbf{Z}_k \in \mathcal{F}(\mathfrak{Z})$, and $\mathbf{Z}_k$ is also a random finite set in $\mathcal{F}(\mathfrak{Z})$.

2) PHD FUNCTIONS

According to [15], the first order moment of the posterior distribution (namely the intensity or PHD) $D(\mathbf{x}|\mathbf{Z})$ is a non-negative function on $\mathfrak{X}$, which can be characterized by

$$\int_{\mathbf{S}} D(\mathbf{x}|\mathbf{Z})d\mathbf{x} = N, \tag{3}$$

where N is the expected number of targets located in $\mathbf{S}$. $\mathbf{S}$, thought as a subset of $\mathfrak{X}$, represents the state set of targets.

Therefore, we can use the intensity $D(\mathbf{x}|\mathbf{Z})$ to estimate the states and number of targets.

C. THE PHD FILTER FOR THE EXTENDED TRACKING

Let $D_{k-1|k-1}(\cdot)$ and $\mathbf{x}_{k-1}$ be the intensity and state of the single extended target at time $k-1$. According to [35], the predicted intensity can be formulated by (4), as shown at the top of the next page. In (4), $p_s(\cdot)$ denotes the survival probability of the single target, $\varphi_{k|k-1}(\cdot)$ is the transition density, $\mathbf{Z}_{1:k-1}$ represents the observation sets from time 1 to $k-1$, and $\gamma(\cdot)$ is the intensity of birth target.

Then, the predicted $D_{k|k-1}(\mathbf{x}_k|\mathbf{Z}_{1:k-1})$ can be updated by

$$D_{k|k}(\mathbf{x}_k) = L_z(\mathbf{x}_k)D_{k|k-1}(\mathbf{x}_k|\mathbf{Z}_{1:k-1}), \tag{5}$$

where $L_z(\cdot)$ represents the pseudolikelihood function, defined by (6), as shown at the top of the next page.

In (6), $\beta(\cdot)$ denotes the expected number of observations generated by single extended target, $c(\cdot)$ is the density of the clutter, $p_D(\cdot)$ is the detection probability of the single target, and $\phi(\mathbf{x}_k)$ is the likelihood of observations generated by a single target. $\mathbf{y}\angle\mathbf{Z}_k$ means that $\mathbf{Z}_k$ is partitioned into nonempty cells W by $\mathbf{y}$. $\mathbf{W}$ is the subset of the current partition, and $\omega_{\mathbf{y}}$ can be considered as the weight of the current partition, expressed by

$$\omega_{\mathbf{y}} = \frac{\prod_{\mathbf{W}\in\mathbf{y}} d_{\mathbf{W}}}{\sum_{\mathbf{y}\angle\mathbf{Z}_k}\prod_{\mathbf{W}} d_{\mathbf{W}}}. \tag{7}$$

The nonnegative coefficient in (7) is represented by (8), as shown at the top of the next page. where $\delta_{i,j}$ is the Kronecker delta.

Equations (4) and (5) describe a PHD recursion in extended target cases. Similar to the standard target cases, there are no closed-forms for (4) and (5).

D. GM-PHD FOR EXTENDED TARGET TRACKING

In this section, we overview the basic idea of the ET-GM-PHD approach. Such an approach can be considered as a Gaussian mixture implementation of the PHD approach in Section II-C. In this approach,the predicted and updated intensities are represented by the GM components. With help of these GM components, (4) and (5) can be changed into the summation of GM components, making these equations tractable. The details of the ET-GM-PHD are provided in the following.

Assume that the state and observation models are subject to linear Gaussian models, represented by

$$\varphi_{k|k-1}(\mathbf{x}_k|\mathbf{x}_{k-1}) \sim N(\mathbf{x}; \mathbf{F}_{k|k-1}\mathbf{x}_{k-1}, \mathbf{Q}_{k-1}) \tag{9}$$

$$\phi_k(\mathbf{z}_k|\mathbf{x}_k) \sim N(\mathbf{z}_k; \mathbf{H}_k\mathbf{x}_k, \mathbf{R}_k) \tag{10}$$

where $\mathbf{F}_{k|k-1}$ is the state transition function, and $\mathbf{H}_k$ is the observation function.

According to [24], the predicted intensity in (4) can be given by

$$D_{k|k-1}(\mathbf{x}) = v_{s,k|k-1}(\mathbf{x}) + \gamma_k(\mathbf{x}), \tag{11}$$

where $v_{s,k|k-1}(\mathbf{x})$ and $\gamma_k(\mathbf{x})$ are the intensities of survival and birth components, respectively. $v_{s,k|k-1}(\mathbf{x})$ is given by

$$v_{s,k|k-1}(\mathbf{x}) = p_{s,k}\sum_{j=1}^{J_{k-1}} w_{k-1}^j N(\mathbf{x}; \mathbf{m}_{k|k-1}^j, \mathbf{P}_{k|k-1}^j), \tag{12}$$

$$D_{k|k-1}(\mathbf{x}_k|\mathbf{Z}_{1:k-1}) = \underbrace{\int_{\mathfrak{X}} p_s(\mathbf{x}_k)\varphi_{k|k-1}(\mathbf{x}_k|\mathbf{x})D_{k-1|k-1}(\mathbf{x}|\mathbf{Z}_{1:k-1})d\mathbf{x}}_{\text{Survival intensity}} + \underbrace{\gamma_k(\mathbf{x}_k)}_{\text{Birth intensity}}, \tag{4}$$

$$L_z(\mathbf{x}_k) = 1 - (1 - e^{\beta(\mathbf{x}_k)})p_D(x_k) + e^{\beta(\mathbf{x}_k)}p_D(\mathbf{x}_k)\sum_{\mathbf{y}\angle\mathbf{Z}_k}\omega_{\mathbf{y}}\sum_{W\angle\mathbf{y}}\frac{\beta(\mathbf{x}_k)^{|\beta(\mathbf{x}_k)|}}{d_W}\cdot\prod_{\mathbf{z}\in\mathbf{W}}\frac{\phi(\mathbf{x}_k)}{\lambda_k c_k(\mathbf{z})}, \tag{6}$$

$$d_{\mathbf{W}} = \delta_{|\mathbf{W}|,1} + \int D_{k|k-1}(\mathbf{x}|\mathbf{Z}_{1:k-1})e^{\beta(\mathbf{x})}\beta(\mathbf{x})^{|\beta(\mathbf{x})|}p_D(\mathbf{x})\prod_{\mathbf{z}\in\mathbf{W}}\frac{\phi(\mathbf{x}_k)}{\lambda_k c_k(\mathbf{z})}d\mathbf{x}, \tag{8}$$

where J_{k-1} is the number of the survival Gaussian mixture components. $\mathbf{m}^j_{k|k-1}$, and $\mathbf{P}^j_{k|k-1}$ denote the predicted state mean and covariance of the j-th component, respectively. In addition, we represent $\gamma_k(\mathbf{x})$ by

$$\gamma_k(\mathbf{x}) = \sum_{i=1}^{J_{r,k}} w^i_{r,k}N(\mathbf{x};\mathbf{m}^i_{r,k},\mathbf{P}^i_{r,k}), \tag{13}$$

where $J_{r,k}$ is the number of birth Gaussian mixture components, and $w^i_{r,k}$ is the weight of the i-th component. $\mathbf{m}^i_{r,k}$ and $\mathbf{P}^i_{r,k}$ denote the mean and covariance, respectively.

Then, the predicted intensity in (11) can be updated by

$$D_{k|k}(\mathbf{x}) = D^{ND}_{k|k}(\mathbf{x}) + D^{D}_{k|k}(\mathbf{x}) \tag{14}$$

where $D^{ND}_{k|k}(\mathbf{x})$ and $D^{D}_{k|k}(\mathbf{x})$ denote the no detection and detected target cases, respectively.

$$D^{ND}_{k|k}(\mathbf{x}) = \sum_{j=1}^{J_{k|k-1}} w^j_{k|k}N(x;\mathbf{m}^j_{k|k},\mathbf{P}^j_{k|k}), \tag{15}$$

$$w^j_{k|k} = (1 - (1 - e^{-\beta(\mathbf{x})}))p_D(\mathbf{x})w^j_{k|k-1}, \tag{16}$$

$$\mathbf{m}^j_{k|k} = \mathbf{m}^j_{k|k-1}, \mathbf{P}^j_{k|k} = \mathbf{P}^j_{k|k-1}, \tag{17}$$

where $\mathbf{m}^j_{k|k}$ and $\mathbf{P}^j_{k|k}$ denote the updated mean and covariance of the j-th component. $w^j_{k|k}$ is the weight of the j-th component.

$$D^{D}_{k|k}(\mathbf{x}) = \sum_{j=1}^{J_{k|k-1}} w^j_{k|k}N(x;\mathbf{m}^j_{k|k},\mathbf{P}^j_{k|k}), \tag{18}$$

$$w^j_{k|k} = \omega_y\frac{\Gamma^j p_D(\mathbf{x})}{d_W}\Phi^j_W w^j_{k|k-1}, \tag{19}$$

$$\Gamma^j = e^{-\beta(\mathbf{x})} - \beta(\mathbf{x})^{|\beta(\mathbf{x})|}, \tag{20}$$

$$\Phi^j_W = \phi^j_{\mathbf{W}}\prod_{\mathbf{z}\in\mathbf{W}}\frac{1}{\lambda_k c_k(\mathbf{z})}. \tag{21}$$

where $\phi^j(\cdot)$ is the likelihood of single target.

Equations (11)-(21) express the main formulations of the ET-GM-PHD approach. Implementing these equations iteratively, the posterior intensities of the extended targets at different time steps can be conveniently achieved. However, according to (9) and (10), the ET-GM-PHD approach assumes the motion and observation models are linear models. Thus, the ET-GM-PHD approach can only handle the linear scenarios. In practice, the motion and observation models are always nonlinear functions. In such scenarios, the ET-GM-PHD approach may lead to great tracking errors.

III. CUBATURE INFORMATION GM-PHD APPROACH FOR EXTENDED TARGET TRACKING

In this section, we present the ET-CISMC-PHD approach in detail. To be more specific, we, first, present a CIF based extended target tracking algorithm in Section III-A. By incorporating the CIF and gating methods into the ET-GM-PHD approach, our ET-CISMC-PHD approach can efficiently estimate states and numbers of extended targets in nonlinear scenarios. For initiating the birth intensity, Section III-B proposes an adaptive intensity initiating method.

A. CIF BASED GM-PHD ALGORITHM FOR EXTENDED TARGET TRACKING

As mentioned in Section II-D, the density $\mathbf{D}_k(\mathbf{x})$ in (14) consists of Gaussian mixture components. The j-th component can be achieved by computing its mean $\mathbf{m}^j_{k|k}$ and covariance $\mathbf{P}^j_{k|k}$. When each pair of $\mathbf{m}^j_{k|k}$ and $\mathbf{P}^j_{k|k}$ are achieved, the density $\mathbf{D}_k(\mathbf{x})$ can be obtained. However, in traditional ET-GM-PHD approach, these components are computed under the linear model. For extending ET-GM-PHD approach into nonlinear scenarios, we utilize the CIF method into our approach for its significant tracking performance in the nonlinear cases. Although the CIF and gating methods have been used in [18], targets of [18] are assumed as the standard targets. Thus, the CIF and gating methods can be directly used. However, in extended target tracking scenarios, these methods cannot be directly used. It is because that these methods are proposed on the standard target assumption. For utilizing these methods into the ET-GM-PHD approach, we use the CIF method to predict states and covariance. The CIF method of [18] uses observations (each observation denotes one possible target) to update predicted observation. In extended target tracking scenarios, each target may generate serval observations. We use the cell to denote observations generated by the same target. For updating the predicted observation of the extended targets by the

CIF method, the cell set should be converted into the observation set. Thus, a gating method has been proposed for extracting the cells associated with the predicted observation of the CIF method. Unlike the standard gating methods (in [12], [14], [18], [36], [37]), our method implements the gating process by computing distances between the predicted observation and cells. Merging the extracted cells into one set, we can construct the observation set for updating the predicted observation of the CIF method. Thus, the CIF method can be used to approximate the states and covariances of the extended targets. Using the approximated states and covariances, the Gaussian mixture components of the ET-GM-PHD approach can be achieved for estimating states of extended targets. Benefitted from the above operations, the tracking performance of the traditional ET-GM-PHD approach in nonlinear scenarios can be significantly improved.

Before introducing our approach, we represent the nonlinear models by

$$\varphi_{k|k-1}(\mathbf{x}_k|\mathbf{x}_{k-1}) \sim N(\mathbf{x}; f(\mathbf{x}_{k-1}), \mathbf{Q}_{k-1}) \tag{22}$$

$$\phi_k(\mathbf{z}_k|\mathbf{x}_k) \sim N(\mathbf{z}_k; h(\mathbf{x}_k), \mathbf{R}_k) \tag{23}$$

where $f(\cdot)$ and $h(\cdot)$ denote the state transition and observation functions, respectively.

In this section, the intensities $v_{s,k|k-1}$ and $D^D_{k|k}(\mathbf{x})$ in (12) and (18) are computed under the nonlinear models (22) and (23). Observed that both of $v_{s,k|k-1}$ and $D^D_{k|k}(\mathbf{x})$ consist of Gaussian components, these Gaussian components can be obtained by computing their means and covariances. Since the models of (22) and (23) are nonlinear functions, we utilize the CIF and gating methods to calculate each pair of the mean and covariance in (12) and (18). For simplicity, we use $\mathbf{m}_{k|k-1}$, $\mathbf{P}_{k|k-1}$, $\mathbf{m}_k$ and $\mathbf{P}_k$ to replace $\mathbf{m}^j_{k|k-1}$, $\mathbf{P}^j_{k|k-1}$, $\mathbf{m}^j_k$ and $\mathbf{P}^j_k$.

Let $\mathbf{W}_i$ be the i-th cell of the current partition. According to Section II-D, our approach consists of *Prediction* and *Update* steps.

Prediction: In this step, we use $\mathbf{m}_{k-1}$ and $\mathbf{P}_{k-1}$ to predict $\mathbf{m}_{k|k-1}$ and $\mathbf{P}_{k|k-1}$. These parameters can be calculated by a group of cubature points. With the achieved $\mathbf{m}_{k|k-1}$ and $\mathbf{P}_{k|k-1}$, the predicted density $v_{s,k|k-1}$ in (12) can be obtained.

According to the cubature rule [38], the n-dimensional Gaussian weighted integral can be approximated by

$$\mathbf{I}_N(c) = \int_{\mathbb{R}^n} c(\mathbf{x})N(\mathbf{x}; \mathbf{m}, \mathbf{P}) \approx \frac{1}{2n}\sum_{j=1}^{2n} c(\mathbf{m} + \sqrt{\mathbf{P}}\boldsymbol{\alpha}_j) \tag{24}$$

where n is the dimension of $\mathbf{m}$,

$$\boldsymbol{\alpha}_j = \sqrt{n}[\mathbf{1}]_j, \quad j = 1, 2, 3, \ldots, 2n \tag{25}$$

and $[\mathbf{1}]_j$ is the j-th vector of the set

$$\left\{ \begin{bmatrix} 1 \\ 0 \\ \vdots \\ 0 \end{bmatrix}, \cdots, \begin{bmatrix} 0 \\ \vdots \\ 0 \\ 1 \end{bmatrix}, \begin{bmatrix} -1 \\ 0 \\ \vdots \\ 0 \end{bmatrix}, \begin{bmatrix} 0 \\ \vdots \\ 0 \\ -1 \end{bmatrix} \right\}.$$

Using the above cubature rule, the $j-$th cubature point at time step $k-1$ can be defined by

$$\boldsymbol{\chi}_{k-1,j} = \sqrt{\mathbf{P}_{k-1}}\boldsymbol{\alpha}_j + \mathbf{m}_{k-1}, \tag{26}$$

Then, the cubature set can be represented by $\{\boldsymbol{\chi}_{k-1,j}\}_{j=1}^{2n}$. Using the cubature set, $\mathbf{m}_{k|k-1}$ and $\mathbf{P}_{k|k-1}$ can be calculated by

$$\mathbf{m}_{k|k-1} = \frac{1}{2n}\sum_{j=1}^{2n} \boldsymbol{\chi}^*_{k-1,j}, \tag{27}$$

$$\mathbf{P}_{k|k-1} = \frac{1}{2n}\sum_{j=1}^{2n} \boldsymbol{\chi}^*_{k-1,j}(\boldsymbol{\chi}^*_{k-1,j})^T - \mathbf{m}_{k|k-1}(\mathbf{m}_{k|k-1})^T + \mathbf{Q}_{k-1}, \tag{28}$$

where $(\cdot)^T$ is the transpose operator, and

$$\boldsymbol{\chi}^*_{k-1,j} = \phi(\boldsymbol{\chi}_{k-1,j}). \tag{29}$$

With the achieved $\mathbf{m}_{k|k-1}$ and $\mathbf{P}_{k|k-1}$, we convert $\mathbf{m}_{k|k-1}$ and $\mathbf{P}_{k|k-1}$ into their information forms,

$$\mathbf{y}_{k|k-1} = \mathbf{Y}_{k|k-1}\mathbf{m}_{k|k-1}, \tag{30}$$

and

$$\mathbf{Y}_{k|k-1} = (\mathbf{P}_{k|k-1})^{-1}, \tag{31}$$

where $\mathbf{y}_{k|k-1}$ and $\mathbf{Y}_{k|k-1}$ denote the information state and matrix, respectively.

By iterating (27) and (28), we compute each pair of $\mathbf{m}^j_{k|k-1}$ and $\mathbf{P}^j_{k|k-1}$ in (12). Thus, the predicted density $v_{s,k|k-1}$ in (12) can be achieved.

Update: With the predicted $\mathbf{y}_{k|k-1}$ and $\mathbf{Y}_{k|k-1}$, we can predict the observation $\mathbf{z}_{k|k-1}$. Then, we update the predicted $\mathbf{z}_{k|k-1}$ by $\{\mathbf{C}_l\}_{l=1}^{N_d}$ (partitioned by Table 1 in [24]). As for the $l-$th partition, several cells may be contained. That means, more than one cells may be used to update $\mathbf{z}_{k|k-1}$. However, the associations between cells and $\mathbf{z}_{k|k-1}$ are hard to be achieved. To tackle with such a problem, we proposed a gating method to extract cells corresponding to $\mathbf{z}_{k|k-1}$. With the extracted cells, we can update $\mathbf{z}_{k|k-1}$. Using the updated $\mathbf{z}_{k|k-1}$, we can calculate $\mathbf{m}_k$ and $\mathbf{P}_k$. Based on the calculated $\mathbf{m}_k$ and $\mathbf{P}_k$, the intensity of (18) can be computed.

The predicted observation $\mathbf{z}_{k|k-1}$ can be denoted by

$$\mathbf{z}_{k|k-1} = \frac{1}{2n}\sum_{j=1}^{2n} \boldsymbol{\chi}^*_{k|k-1,j}, \tag{32}$$

where

$$\boldsymbol{\chi}^*_{k|k-1,j} = \varphi(\boldsymbol{\chi}_{k|k-1,j}), \tag{33}$$

and

$$\boldsymbol{\chi}_{k|k-1,j} = \sqrt{\mathbf{P}_{k|k-1}}\boldsymbol{\alpha}_j + \boldsymbol{m}_{k|k-1}. \tag{34}$$

Using the denoted $\mathbf{z}_{k|k-1}$ of (32), we can evaluate the cross covariance matrix of state and observation by (35), as shown at the top of the next page.

$$\mathbf{P}^{mz}_{k|k-1} = \frac{1}{2n}\sum_{j=1}^{2n}(\boldsymbol{\chi}_{k|k-1,j} - \boldsymbol{m}_{k|k-1})(\boldsymbol{\chi}^{*}_{k|k-1,j} - \mathbf{z}_{k|k-1})^{T} = \frac{1}{2n}\sum_{j=1}^{2n}\boldsymbol{\chi}_{k|k-1,j}(\boldsymbol{\chi}^{*}_{k|k-1,j})^{T} - \boldsymbol{m}_{k|k-1}(\mathbf{z}_{k|k-1})^{T}. \tag{35}$$

Then, the state contribution and its corresponding information matrix can be computed by

$$\mathbf{i}_{k,j} = \mathbf{Y_{k|k-1}}\mathbf{P}^{mz}_{k|k-1}\mathbf{R}_{k}^{-1}(\boldsymbol{\mu}_{j} + (\mathbf{Y_{k|k-1}}\mathbf{P}^{mz}_{k|k-1})^{T}\mathbf{m}_{k|k-1}), \tag{36}$$

and

$$\mathbf{I}_{k} = \mathbf{Y_{k|k-1}}\mathbf{P}^{mz}_{k|k-1}\mathbf{R}_{k}^{-1}(\mathbf{Y_{k|k-1}}\mathbf{P}^{mz}_{k|k-1})^{T}, \tag{37}$$

where $\boldsymbol{\mu}_j$ represents the innovation of the j-th observation $\mathbf{z}_j$

$$\boldsymbol{\mu}_{j} = \mathbf{z}_{j} - \mathbf{z}_{k|k-1}. \tag{38}$$

Here, $\mathbf{z}_j$ is the $j-$th component of the observation set $\tilde{\mathbf{Z}}_k$, and $\tilde{\mathbf{Z}}_k$ represents the observation set of the current target. We also assume that $\mathbf{z}_j$ is a two-dimension vector, and $\boldsymbol{\mu}_j$ follows a two-dimension Gaussian distribution.

Thus, we can obtain the information state vector $\mathbf{y}_k$ and matrix $\mathbf{Y}_k$ by

$$\mathbf{y}_{k} = \mathbf{y}_{k|k-1} + \sum_{j=1}^{N_l}\mathbf{i}_{k,j}, \tag{39}$$

$$\mathbf{Y}_{k} = \mathbf{Y}_{k|k-1} + \sum_{j=1}^{N_l}\mathbf{I}_{k,j}. \tag{40}$$

where N_l is the number of observations, $N_l = |\tilde{\mathbf{Z}}_k|$.

Equations (38)-(40) have been proposed in standard target tracking scenarios. In extended target tracking scenarios, observations generated by the same target are represented by the cell. For applying these equations into extended target tracking scenarios, we utilize the gating method into the CIF method for constructing $\tilde{\mathbf{Z}}_k$. Unlike the traditional gating methods in [12], [14], [18], [36], [37], our method directly implement on cells, leading to small computational cost. Our gating method method consists of two steps.

Step 1 Extract candidate cells from the current partition

In this paper, we use the center to represent the current cell. Then, we compute the distances between the predicted observation and cells of the current partition. By selecting certain threshold for these distances, the candidate cells can be extracted.

Let $\mathbf{z}_{c,i}$ denote the center of the cell $\mathbf{W}_i$,

$$\mathbf{z}_{c,i} = \frac{1}{|\mathbf{W}_i|}\sum_{j=1}^{|\mathbf{W}_i|}\mathbf{z}_{j}, \tag{41}$$

where $\mathbf{z}_j \in \mathbf{W}_i$.

The distance between cell $\mathbf{W}_i$ and $\mathbf{z}_{k|k-1}$ can be defined by

$$d(\mathbf{z}_{k|k-1}, \mathbf{z}^{i}_{c}) = \sqrt{(\mathbf{z}_{k|k-1} - \mathbf{z}^{i}_{c})^{T}\mathbf{R}^{-1}(\mathbf{z}_{k|k-1} - \mathbf{z}^{i}_{c})}, \tag{42}$$

Using (42), the candidate cells can be computed by

$$\tilde{\mathbf{W}}_{k} = \{\mathbf{W}_{i} | d(\mathbf{z}_{k|k-1}, \mathbf{z}^{i}_{c}) < T_{h}\}, \tag{43}$$

where T_h is the threshold.

Step 2 Constructing observation set associated with the target.

Let $\tilde{\mathbf{W}}_i$ be the i-th cell of the candidate cell set $\tilde{\mathbf{W}}_k$. According to (38)-(40), the observation set (consists of possible observations) are used for updating the predicted observation. Thus, the candidate cells must be merged into one observation set. We merge the candidate cells by

$$\tilde{\mathbf{Z}}_{k} = \{\mathbf{z} | \mathbf{z} \in \tilde{\mathbf{W}}_{i}, i = 1, 2, \ldots, N_l\}, \tag{44}$$

where, $N_l = \sum_{i=1}^{|\tilde{\mathbf{W}}_k|}|\tilde{\mathbf{W}}_i|$.

Substituting $\tilde{\mathbf{Z}}_k$ into (38)-(40), we can obtain $\mathbf{y}_k$ and $\mathbf{Y}_k$. Then, the posterior state $\mathbf{m}_k$ and $\mathbf{P}_k$ can be constructed based on (30) and (46), given by:

$$\mathbf{m}_{k} = \mathbf{Y}_{k}{}^{-1}\mathbf{y}_{k}, \tag{45}$$

$$\mathbf{P}_{k} = (\mathbf{Y}_{k})^{-1}. \tag{46}$$

When there is no cells in the current gate ($\tilde{\mathbf{W}}_k = \emptyset$), $\mathbf{m}_k$ and $\mathbf{P}_k$ can be approximated in the following:

$$\mathbf{m}_{k} = \mathbf{m}_{k|k-1}, \tag{47}$$

$$\mathbf{P}_{k} = \mathbf{P}_{k|k-1}. \tag{48}$$

Substituting $\mathbf{m}_k$ and $\mathbf{P}_k$ into (18)-(21), we can finally achieve the posterior intensity of our approach.

B. BIRTH INTENSITY INITIATION METHOD

According to (4), the predicted intensity consists of birth and survival intensities. Commonly, the birth intensity is known as a prior. However, it is unavailable in practice. Besides, the observation set of multi extended targets are also partitioned into several possible partitions. When the number of partitions are large, directly using all of the partitions for birth intensity initiation may cost great computational time. Moreover, each partition of the multi extended targets consists of cells. As for each cell, several observations are contained in it. Thus, the adaptive birth intensity methods of standard target tracking can not be adopted in multi extended target tracking. In this paper, we propose an observation driven birth intensity initiating method for the birth intensity initiation. To be more specific, we, first, project states of estimated targets into the observation space. After projection, we compute distances between the projected observations and cell centers of partitions. By setting certain threshold, we can calculate the number of cells corresponding to the estimated targets for each partition. Second, we select the

partition with the largest number as the most possible partition. With the selected partition, we remove the survival cells from the ''real'' partition. The left cells can be considered as the observations generated by the birth targets. Third, we define the contribution factor to measure the degree of importance of the current component to its corresponding cell. By computing the contribution factors, we can achieve the Gaussian components of the birth intensity. With these three steps, the birth intensity can be initiated for the next recursion.

Before introducing our method, we represent the projecting model for mapping the observation into the state space. Here, we use the bearing and range model [39] to illustrate our method. Remember that, $\mathbf{x}_k$ and $\mathbf{z}_k$ are the state and observation at time step k, respectively. Assume that r_k and θ_k denote the different dimensions of $\mathbf{z}_k$, where r_k is the range dimension, and θ_k represents the angle dimension. Then, according to the unbiased model of [40], the projecting model for mapping the state into the observation space can be given as follows

$$u_k^x = \beta_\theta^{-1} r_{k,i} \cos\theta_k, \tag{49}$$

$$u_k^y = \beta_\theta^{-1} r_{k,i} \sin\theta_{k,i}, \tag{50}$$

where (u_k^x, u_k^y) denotes the position coordinate of $\mathbf{x}_k$. β_θ is the biased comparison factor, $\beta_\theta = \sigma_\theta$, where σ_θ, given as a prior, represents the error of bearing angle θ_k.

Let $\mathbf{M}_i$ be the $i-$th cell of the current projected partition $\mathbf{G}$, and $\mathbf{m}$ be the center of $\mathbf{M}_i$. According to (49), we define the distance between $\mathbf{M}_i$ and $\mathbf{x}$ by

$$d_{\mathbf{E}_i,\mathbf{x}} = \left\| \bar{u} - \begin{bmatrix} 1 & 0 & 0 & 0 & 0 \\ 0 & 0 & 1 & 0 & 0 \end{bmatrix} \mathbf{x} \right\|, \tag{51}$$

where $\|\cdot\|$ represents the ℓ_2-norm. In the following, we utilize (51) for extracting the candidate cells.

Step1 (Find the Partition of Current Targets, and Remove Cells Associated With the Estimated Targets):

Recall Section II-A, an extended target may generate more than one observations. Thus, in multi extended target tracking scenarios, we can cluster the observations into several cells. However, the associations between states and observations are commonly unknown. We can only achieve all of the possible partitions under the current observation set. Obviously, cells with small distances may have large probability to be generated by the estimated targets. Thus, we can use (51) to find cells associated with the estimated set in the current partition. By setting certain thresholds, we can achieve the cells associated with the estimated target set. Then, we count the cell number for each partition. The partition that has the largest number can be considered as the partition that survival targets belong to. Meantime, we remove the cells associated with the estimated targets. The left cells can be considered as cells of the birth targets. At last, we use the contribution factors to compute the birth intensity.

Let $\mathbf{X}_k^e$ be the state set of estimated targets, $\tilde{\mathbf{C}}_k$ be the projected partition of birth targets, $\mathbf{U}_k$ be the mapped set of $\mathbf{Z}_k$, and $\mathbf{G}_l$ be the $l-$th partition of $\mathbf{U}_k$. With the help of the distance of (51), we can obtain the candidate partition of birth targets using the procedure in Table 1.

Step2: Estimate the components of birth targets.

Once the candidate cell set $\mathbf{C}_k^b$ has been achieved, we turn to estimate the birth components (the mean of the $i-$th target state vector $\mathbf{m}_{k,i}$ and its corresponding covariance $\mathbf{P}_{k,i}$) by the unbiased model of [40].

Recall that each cell may contain more than one observation, in other words, there are more than one elements for each cell of $\mathbf{C}_k^b$. In order to combine these elements into one element, we tend to use (51) to compute the distance between each element and its corresponding cell. Let $\mathbf{u}_{k,j}$ and $\mathbf{u}_{k,c}$ be the $j-$th element and its corresponding cell center, d_j be the distance between $\mathbf{u}_{k,j}$ and $\mathbf{u}_{k,c}$, where d_j can be computed by (51). We define the contribution factor (denoting the contribution of $\mathbf{u}_{k,j}^z$ to its corresponding cell) as

$$s_j = \frac{D_j}{\sum_{j=1}^{N_b} D_j}, \tag{52}$$

where

$$D_j = \frac{1}{d_j / \max_j d_j}, \tag{53}$$

and N_b is the number of current cells.

Using (52), we combine element of $i-$th cell into one element by

$$\mathbf{t}_{k,i} = \sum_{j=1}^{N_d^i} s_j^i * \mathbf{u}_{k,j}, \tag{54}$$

where i denotes the $i-$th cell.

Let $p_{k,i}^x$ and $p_{k,i}^y$ be the two dimensions of $\mathbf{t}_{k,i}$, the mean of the $i-$th new born target is defined by

$$\mathbf{m}_k^{(i)} = [p_{k,i}^x, 0, p_{k,i}^y, 0, 0]^T. \tag{55}$$

The covariance can be estimated by

$$\mathbf{P}_k^{(i)} = \begin{bmatrix} \sigma_{xx} & 0 & \sigma_{xy} & 0 & 0 \\ 0 & \sigma_v & 0 & 0 & 0 \\ \sigma_{yy} & 0 & \sigma_{xy} & 0 & 0 \\ 0 & 0 & 0 & \sigma_v^2 & 0 \\ 0 & 0 & 0 & 0 & \sigma_\theta^2 \end{bmatrix}, \tag{56}$$

where σ_v is the standard deviation of velocity known as a prior. In (56), the following exists:

$$\begin{cases} \sigma_{xx} = (\beta_\theta^{-2} - 2)(\tilde{r}_{k,i})^2 \cos^2(\theta_{k,i}) + 0.5((\tilde{r}_{k,i})^2 \\ \quad +\sigma_r^2)(1 + \beta_\theta^4 \cos(2\theta_{k,i})) \\ \sigma_{xy} = (\beta_\theta^{-2} - 2)(\tilde{r}_{k,i})^2 \cos(\theta_{k,i}) \sin(\theta_{k,i}) + 0.5((\tilde{r}_{k,i})^2 \\ \quad +\sigma_r^2)(1 + \beta_\theta^4 \cos(2\theta_{k,i})) \\ \sigma_{yy} = (\beta_\theta^{-2} - 2)(\tilde{r}_{k,i})^2 \sin^2(\theta_{k,i}) + 0.5((\tilde{r}_{k,i})^2 \\ \quad +\sigma_r^2)(1 - \beta_\theta^4 \cos(2\theta_{k,i})). \end{cases} \tag{57}$$

Finally, the new born targets can be constructed by $\{\mathbf{m}_{k,i}, \mathbf{P}_{k,i}\}_{i=1}^{N_k^b}$. At time $k+1$, the CIF (discussed in Section III-A) are used to achieve birth intensity of (13). We summarize our ET-CIGM-PHD approach in Table 2.

TABLE 1. Finding partitions and removing cells associated with the estimated targets.

- **Input:** Observation set $\mathbf{Z}_k$, partition set $\{\mathbf{C}_l\}_{l=1}^{N_d}$ and estimated state set $\mathbf{X}_k^e$.
- **Output:** Projected partition of birth targets $\mathbf{C}_k^b$.
  - Project the observation set $\mathbf{Z}_k$ into its state form $\mathbf{U}_k$ by (49) and (50).
  - Cluster $\mathbf{U}_k$ into its partition set $\{\mathbf{G}_l\}_{l=1}^{N_d}$ according to $\{\mathbf{C}_l\}_{l=1}^{N_d}$.
  - **For:** $l = 1, 2, \cdots, N_d$,
    - **For:** $j = 1, 2, \cdots, |\mathbf{X}_k^e|$,
      1 Compute the distance $d_{\mathbf{M}_{i,l},\tilde{\mathbf{x}}_{k,j}}$ by (51), where $\tilde{\mathbf{x}}_{k,j}$ is the $j-$th state of $\mathbf{X}_k^e$, and $i = 1, 2, \cdots, |\mathbf{G}_l|$.
      2 Extract the candidate cell $\mathbf{V}_j$ satisfying $\mathbf{V}_j = \arg\min_{\mathbf{M}_{i,l}} d_{\mathbf{M}_{i,l},\tilde{\mathbf{x}}_{k,j}}$ *s.t.* $d_{\mathbf{M}_{i,l},\tilde{\mathbf{x}}_{k,j}} <= l * \sigma_r$. Here, we set $l = 4$.
    - **End For**
  - Construct the $l-$th candidate partition $\mathbf{A}_l$ by $\mathbf{A}_l = \{\mathbf{V}_j\}_{j=1}^{|\mathbf{X}_k^e|}$.
  - **End For**
  - Estimate the candidate survival cells $\tilde{\mathbf{A}}$ by $\tilde{\mathbf{A}} = \arg\max_{\mathbf{A}_l} N_l$, where N_l is the number of nonempty cells of $\mathbf{A}_l$. Here, we use $\tilde{\mathbf{C}}$ to denote the partition that $\tilde{\mathbf{A}}$ belongs to.
  - Calculate the projected partition of birth targets by $\mathbf{C}_k^b = \tilde{\mathbf{C}} \backslash \tilde{\mathbf{A}}$.
  - Return $\mathbf{C}_k^b$.

TABLE 2. The ET-CIGM-PHD approach from time step $k-1$ to k.

- **Input:** Birth component $\mathbf{B}_{k-1}$, survival component set $\{x_{k-1}^{(i)}, \mathbf{P}_{k-1}^{(i)}, w_{k-1}^{(i)}\}_{i=1}^{L_{k-1}}$, and current observation set $\mathbf{Z}_k$
- **Output:** Target number N_k, birth component $\mathbf{B}_k$, and estimated state set $\mathbf{X}_k^e$
  - Cluster $\mathbf{Z}_k$ into N_d candidate partitions by Table I in [24]. Here we use $\{\mathbf{C}_l\}_{l=1}^{N_d}$ to represent the partition set.
  - Calculate the survival intensity $v_{s,k|k-1}(\mathbf{x})$ of (12) by (27)-(28).
  - Approximate the birth intensity $\gamma_k(\mathbf{x})$ of (13) by (27)-(28).
  - Substitute $v_{s,k|k-1}(\mathbf{x})$ and $\gamma_k(\mathbf{x})$ into (11) to achieve the predicted intensity $D_{k|k-1}(\mathbf{x})$.
  - Update the intensity of (18) by (45)-(46).
  - Prune the GM components by Table II in [39]. The remaining components $\{x_{k-1}^{(i)}, \mathbf{P}_{k-1}^{(i)}, w_{k-1}^{(i)}\}_{i=1}^{L_{k-1}}$ can be considered as the survival components at next time step.
  - Extract the estimated target set $\mathbf{X}_k^e$, and compute the target number M_k.
  - Find partitions, and remove cells associated with $\mathbf{X}_k^e$ by Table 1 in Section III-B.
  - Utilize the remaining set $\mathbf{C}_k^b$ to obtain the birth $\mathbf{B}_k$ by (55) and (56).
  - Return N_k, $\mathbf{X}_k^e$ and $\mathbf{B}_k$.

IV. SIMULATION RESULTS

In this section, we validate performance of the proposed ET-CIGM-PHD approach. A simulation scenario composed of five targets is constructed in Section IV-A. Under such a scenario, we compare the tracking errors of the ET-GM-PHD [24], CK-EPHD [25] and our ET-CIGM-PHD approaches in terms of the optimal subpattern assignment (OSPA) metric [41] and Root Mean Square Error (RMSE) in Section IV-C. We follow the way of [24] and [25] to compare OSPA distances and RMSE of the estimated targets. Finally, we compare the simulation results of these approaches with different numbers of clutters and detection probabilities, to prove the effectiveness of our approach.

A. SIMULATION SCENARIOS

In our simulations, we adopt the nonlinear scenarios of [18]. For simplicity, we define the target states $\mathbf{x}$ by $\mathbf{x} = [p_x, v_x, p_y, v_y, \alpha]^T$. In this paper, (p_x, p_y) is the vector of the position, (v_x, v_y) is the vector of the velocity, and α is the turn rate. Using these definitions, we represent the nonlinear dynamic model as

$$\begin{aligned}\mathbf{x}_k &= \begin{bmatrix} 1 & \frac{\sin(\alpha_{k-1}T)}{\alpha_{k-1}} & 0 & -\frac{1-\cos(\alpha_{k-1}T)}{\alpha_{k-1}} & 0 \\ 0 & \cos(\alpha_{k-1}T) & 0 & -\sin(\alpha_{k-1}T) & 0 \\ 0 & \frac{1-\cos(\alpha_{k-1}T)}{\alpha_{k-1}} & 1 & \frac{\sin(\alpha_{k-1}T)}{\alpha_{k-1}} & 0 \\ 0 & \sin(\alpha_{k-1}T) & 0 & \cos(\alpha_{k-1}T) & 0 \\ 0 & 0 & 0 & 0 & 1 \end{bmatrix} \\ &\quad \times \mathbf{x}_{k-1} + \begin{bmatrix} \frac{T^2}{2} & 0 & 0 \\ T & 0 & 0 \\ 0 & \frac{T^2}{2} & 0 \\ 0 & T & 0 \\ 0 & 0 & 1 \end{bmatrix} \boldsymbol{\varepsilon}_{k-1}, \end{aligned} \tag{58}$$

TABLE 3. The initial state of the targets.

	state	appear time(s)	disappear time(s)
Target1	$[400\text{m}, 5\text{m/s}, 400\text{m}, 5\text{m/s}, 0\text{rad/s}]$	1	40
Target2	$[440\text{m}, -5\text{m/s}, 440\text{m}, 5\text{m/s}, 0\text{rad/s}]$	8	50
Target3	$[350\text{m}, 5\text{m/s}, 350\text{m}, -5\text{m/s}, 0\text{rad/s}]$	25	70
Target4	$[425\text{m}, 5\text{m/s}, 375\text{m}, -5\text{m/s}, 0\text{rad/s}]$	59	70
Target5	$[375\text{m}, -5\text{m/s}, 425\text{m}, 5\text{m/s}, 0\text{rad/s}]$	59	70

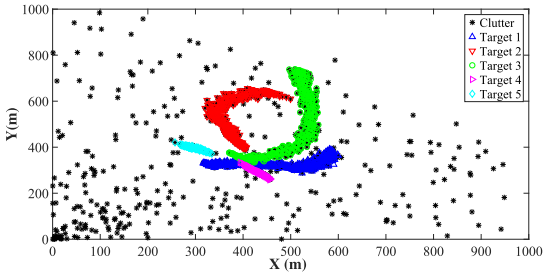

FIGURE 3. Ground-truth trajectories of five targets with the clutter number setting to be 20. The target trajectories are depicted by circle-solid lines with different colors, while the asterisks denote clutters.

where $T = 1$ second (s) is the sampling interval, and $\boldsymbol{\varepsilon}_{k-1}$ is the noise defined by $\boldsymbol{\varepsilon}_{k-1} \sim N(\boldsymbol{\varepsilon}_{k-1}; 0, \mathbf{Q})$. Here, $\mathbf{Q} = diag(\sigma^2_{x,\boldsymbol{\varepsilon}}, \sigma^2_{y,\varepsilon}, \sigma^2_{\alpha})$ denotes the covariance matrix of $\boldsymbol{\varepsilon}_{k-1}$. In addition, we set $\sigma_{x,\varepsilon} = \sigma_{y,\boldsymbol{\varepsilon}} = 1$ meter/second^2 (m/s^2), and $\sigma_{\alpha} = \pi/180$ rad. The initial states of the five targets are listed in Table 3.

Besides, we use the observation model as follows,

$$\mathbf{z}_k = \begin{bmatrix} \arctan\left(\dfrac{p_y}{p_x}\right) \\ \sqrt{p_x^2 + p_y^2} \end{bmatrix} + \boldsymbol{\eta}_k, \tag{59}$$

where, $\eta_k \sim N(\cdot; 0, \mathbf{R})$ represents the observation noise, and $\mathbf{R}$ is the covariance defined by $\mathbf{R} = diag(\sigma_{\theta}^2, \sigma_r^2)$. In this paper, we set $\sigma_{\theta} = \frac{\pi}{180}$ rad and $\sigma_r = 1$ m. Moveover, we assume that the clutter follows the uniform distribution in the detection region. The angle range and distance range of the detection region are $(0, \pi/2)$ rad and $(0, 1000)$ m, respectively. Using the above parameters, the trajectories of the five targets are shown in Figure 3.

For parameters, we set the gating threshold $T_h = 4$ according to [42]. The probabilities of survival and detection are $p_s = 0.99$ and $p_d = 0.95$ in accordance with [39]. All of the simulations are run in the environment with MATLAB2016a, and i7 processor with 8GB RAM.

In order to validate the estimation accuracy, we select the second order OSPA distance and RMSE as the metric. Before comparison, we represent the basic idea of the second order OSPA as follows. Let $\mathbf{X} = \{\mathbf{x}_1, \ldots, \mathbf{x}_m\}$ and $\mathbf{Y} = \{\mathbf{Y}_1, \ldots, \mathbf{Y}_n\}$ be two RFSs. m and n denote the numbers of elements in $\mathbf{X}$ and $\mathbf{Y}$, respectively. Let Ω_n be the set of permutations of $\{1, 2, \ldots, m\}$, the second order OSPA distance

TABLE 4. The estimated results of the ET-CIGM-PHD under different thresholds.

Thresholds	OSPA (m)	RMSE
2	16.22	0.34
3	9.62	0.15
4	9.10	0.14
5	9.12	0.14

can be represented by

$$\bar{d}^c(\mathbf{X}, \mathbf{Y}) = \frac{1}{n}\left(\min_{\varsigma \in \Omega_n} \sum_{i=1}^{m} d^c(\mathbf{x}_i, \mathbf{y}_{\varsigma(i)})^2 + c^2(n-m)\right)^{\frac{1}{2}}, \tag{60}$$

where $d^c(\mathbf{x}, \mathbf{y}) = \min(c, d(\mathbf{x}, \mathbf{y}))$, $c > 0$ is a cut off factor, and $d(\mathbf{x}, \mathbf{y})$ is the distance between $\mathbf{x}$ and $\mathbf{y}$. Here, we adopt the Euclidean distance to calculate $d(\mathbf{x}, \mathbf{y})$. In this paper, we assume that the value of c is equal to 70.

B. COMPARISON OF ESTIMATION ACCURACY ON DIFFERENT THRESHOLDS

To validate the influence of thresholds, we implement the ET-CIGM-PHD approach under different thresholds. Here, we select the following values $T_h = 2, 3, 4, 5$. According to the definition of χ^2 distribution, these values represent that the probabilities of the observation locating in the gate are set to be 87%, 98.9%, 99.9% and 100%. For each value, the ET-CIGM-PHD is performed with 500 Monte Carlo runs. The estimated results are listed in Table 4.

When the possibility is small, the observations generated by the target may not be located in the gate. When the possibility is large, more clutters may be contained in the gating. Both of cases may lead to the large tracking errors. According to this, in Table 4, we can observe that the estimated results of $T_h = 4$ is the smallest in all of the selected thresholds. Thus, in this section, we select $T_h = 4$ in the following simulations.

C. COMPARISON OF ESTIMATION ACCURACY ON CERTAIN NUMBER OF CLUTTERS

Under the above parameters, all of these three approaches are implemented with 500 Monte Carlo runs. For justice, all of these approaches utilize the birth intensity initiating method of Section III-B. The estimated trajectories are demonstrated in Figure 4 to 6. From these figures, we can observe that the estimated points of CK-EPHD and our ET-CIGM-PHD approaches are rather closer to the true trajectories

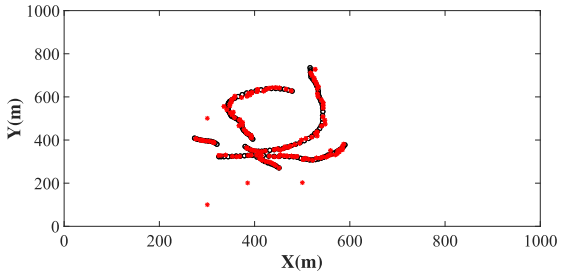

FIGURE 4. Estimated trajectories of ET-GM-PHD. We use the red (light) points to represent the estimated trajectories, while the the true trajectories denote the black (dark) solid lines.

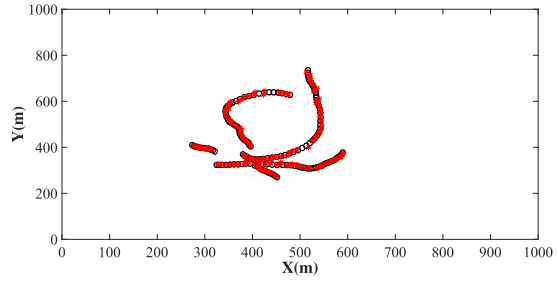

FIGURE 5. Estimated Trajectories of CK-EPHD. We use the red (light) points to represent the estimated trajectories, while the the true trajectories denote the black (dark) solid lines.

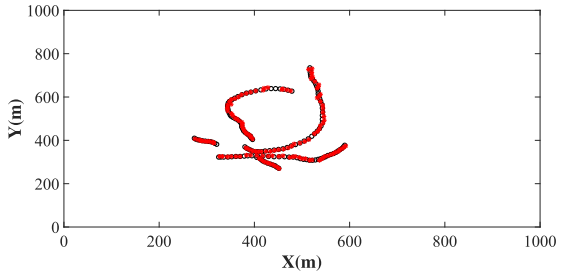

FIGURE 6. Estimated trajectories of ET-CIGM-PHD. We use the red (light) points to represent the estimated trajectories, while the the true trajectories denote the black (dark) solid lines.

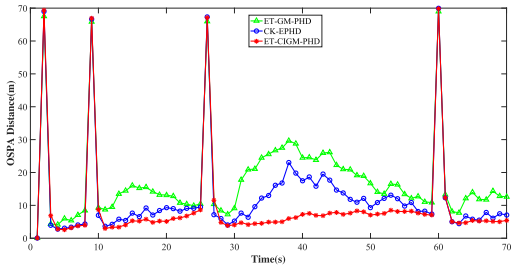

FIGURE 7. OSPA distances of the ET-GM-PHD, CK-EPHD and ET-CIGM-PHD approaches with clutter number being 20.

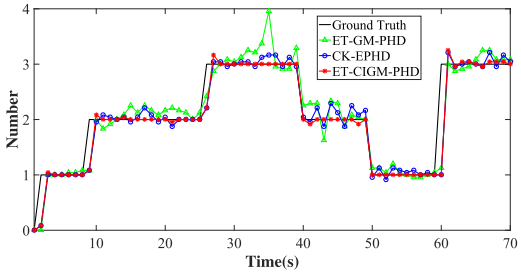

FIGURE 8. Estimated numbers of three approaches with clutter number being 20.

than the ET-GM-PHD approach. Moreover, compared with Figure 4 and 5, most of the estimated points in Figure 6 are overlapped with the true trajectories.

In order to compare the estimated performance of the above approaches, we demonstrate the OSPA distances in Figure 7. Here, we use the averaged OSPA distances and RMSEs of all three approaches. Here, the averaged OSPA distance refers to the average of OSPA distances among 500 Monte Carlo runs. From Figure 7, we can observe that the OSPA distance of the ET-GM-PHD approach is largest in all of these three approaches. Noted that larger OSPA distance corresponds to the larger tracking error, the ET-GM-PHD approach has larger tracking error than the CK-EPHD and our ET-CIGM-PHD approaches. This is because the CK-EPHD and proposed ET-CIGM-PHD approaches utilize the CKF and CIF methods to improve the tracking performance of the ET-GM-PHD approach,respectively. Due to the significant tracking performance of the CKF and CIF methods, these two approaches have better tracking accuracy than the ET-GM-PHD approach. In addition, we can also observe that the proposed ET-CIGM-PHD approach has smallest OSPA distance in all of these approaches.

To further validate the tracking performance, we provide the estimated numbers and RMSEs of these three approaches in Figure 8 and 9. The number in Figure 8 refers to the target number. From Figure 8, we can observe that most of the estimated numbers of the ET-CIGM-PHD approach are located around the ground truth. That means, the ET-CIGM-PHD approach has better accuracy for estimating the number of target than the other two approaches. It is because that we integrate CIF and gating methods into the ET-GM-PHD. For the high tracking performance of the CIF, the estimated numbers of the proposed approach are more accurate than the ET-GM-PHD and CK-EPHD. Figure 9 depicts the RMSEs of the three approaches. From this figure, we can observe that the RMSE of the ET-CIGM-PHD approach is the smallest. That means, the estimated number of the ET-CIGM-PHD approach is the most accurate in all of these approaches. That is because we utilize the CIF method and gating method to compute the Gaussian mixture components. Since cells that have large probability to be generated by the clutter have been removed from the current partition, the estimated results of our approach are more accurate than the ET-GM-PHD and CK-EPHD approaches.

Moreover, we list the numerical results of both approaches in Table 5. According to Table 5, the CK-EPHD approach has the longest computational time, while the proposed ET-CIGM-PHD approach has the shortest computational time. This is because the CK-EPHD approach costs a lot of

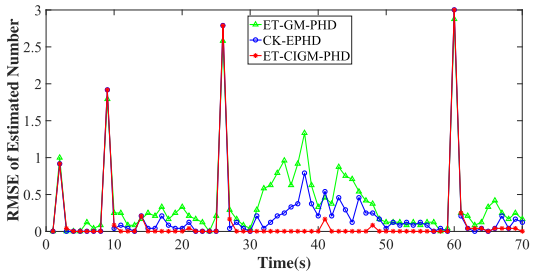

FIGURE 9. RMSEs of the three approaches with clutter number being 20.

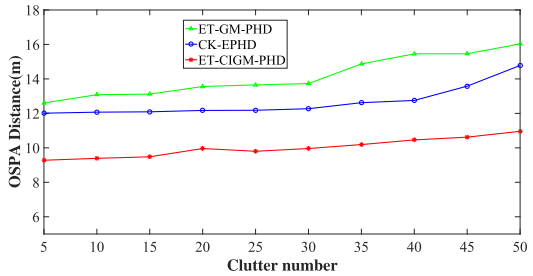

FIGURE 10. Averaged OSPA distances of the ET-GM-PHD, CK-EPHD and our ET-CIGM-PHD approaches along with the clutter number changing from 5 to 50.

TABLE 5. Averaged estimation errors and computational times per target.

Approaches	OSPA (m)	RMSE	Time (ms)
ET-GM-PHD	14.43	0.39	0.02
CK-EPHD	12.62	0.26	0.06
ET-CIGM-PHD	9.96	0.15	0.01

time to predict and update the cubature points, leading to longer time than the ET-GM-PHD approach. However, in our ET-CIGM-PHD approach, we select the CIF to estimate the Gaussian mixture components. The update stage of the CIF method is more computationally economic than the CKF method. Besides, we only select part of cells to update the predicted observations for reducing computational complexity. Thus, the computation load can be significantly reduced.

D. COMPARISON OF ESTIMATION ACCURACY ON VARIOUS NUMBER OF CLUTTERS

To validate the effect of clutters, we change the number of clutters ranging from 5 to 50. For each number of clutters, the ET-GM-PHD, CK-EPHD and our ET-CIGM-PHD approaches are performed with 500 Monte Carlo runs. We plot the estimated results of these approaches in Figure 10 and 11. Figure 10 demonstrates the mean OSPA distances on various number of clutters, and the averaged RMSEs are plotted in Figure 11. Due to the significant tracking performance of the CKF and CIF methods, the CK-EPHD and our ET-CIGM-PHD approaches have better tracking accuracy than the ET-GM-PHD approach (seen in Figure 10 and 11). We can also observed that the mean OSPA distances and RMSEs of the proposed ET-CIGM-PHD approach are smallest in all of three approaches in Figure 10 and 11. Since clutters outside the selected gate have been removed in the update stage, the estimated results of our approach in Figure 10 and 11 are more stable than the other two.

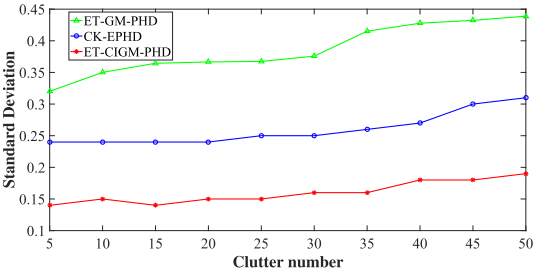

FIGURE 11. Averaged RMSEs of estimated number of the ET-GM-PHD, CK-EPHD and our ET-CIGM-PHD approaches along with the clutter number changing from 5 to 50.

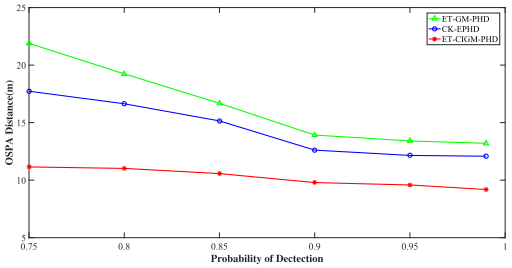

FIGURE 12. Averaged OSPA distances of the ET-GM-PHD, CK-EPHD and our ET-CIGM-PHD approaches along with the probability of detection changing from 0.75 to 0.99.

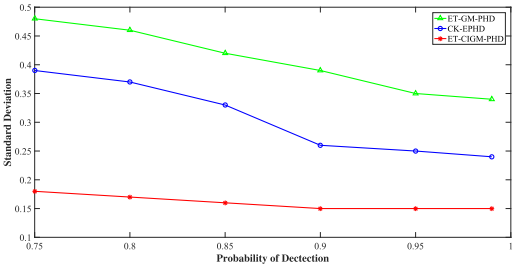

FIGURE 13. Averaged RMSEs of estimated number of the ET-GM-PHD, CK-EPHD and our ET-CIGM-PHD approaches along with the probability of detection changing from 0.75 to 0.99.

E. COMPARISON OF ESTIMATION ACCURACY ON DIFFERENT PROBABILITIES OF DETECTION

In this section, we implement the ET-GM-PHD, CK-EPHD and proposed ET-CIGM-PHD approaches under different probabilities of detection (varying from 0.75 to 0.99). All of these approaches have been simulated with 500 Monte Carlo runs. Here, we set the number of clutters to be 20. We plot the results in Figure 12 and 13. From these figures, we can observe that when the probability of detection is less than 0.95, the OSPA distances and RMSEs are rapidly reduced. When the probability increases from 0.95 to 0.99, the OSPA distances and RMSEs are reduced slowly. The reason is that

when the probability grows large, many observations generated by targets are detected. Thus, the tracking accuracy of the three approaches becomes better. Along with the growing probability, the estimated results of these approaches tend to be stable. In addition, using the CIF and gating methods, the OSPA distances and RMSEs of the proposed approach are smaller than the ET-GM-PHD and CK-EPHD approaches, enjoying the best estimated accuracy.

V. CONCLUSION

In this paper, we have proposed the ET-CIGM-PHD approach, which can be applied to estimate the number and states of multi extended targets in nonlinear scenarios. In our approach, we utilize the CIF to approximate the GM components of targets for its significant tracking accuracy in nonlinear scenarios. In order to construct the observation set, and reduce the computation complexity, we present a gating method to extract the cells associated with the predicted observation. Then, these abstracted cells are combined into one set for updating the predicted observation of the CIF method. Since our method directly implements the gating process on the cells. Thus, the tracking performance of the traditional ET-GM-PHD approach can be significantly improved. Moreover, we propose an adaptive initiation method for birth component initiating. Using the estimated states into initiation, the proposed approach can initiate the birth intensity adaptively. The simulation results demonstrate that our ET-CIGM-PHD approach outperforms the ET-GM-PHD and CK-EPHD approaches in terms of tracking accuracy.

This paper focuses on improving the efficiency and accuracy of the traditional ET-GM-PHD approach. It simply uses the GM component pruning and state estimating methods. Other component pruning, state estimating, and clustering methods may be incorporated into the future work. Studying on optimizing parameters of observation partitioning can be seen as another direction of the future work. In addition, for lack of equipment and data sets, we verify our approach with simulation data. Experiments with measured data will be the third direction of the future work.

APPENDIX A
DERIVATIVES OF $\omega_{\mathbf{Y}}$

In this section, we give the proof of $\omega_{\mathbf{y}}$ in (7), which has been derived in [1].

According to [1], the extended target posterior probability-generating function (*p.g.fl.*) $G_{k+1|k+1}[h]$ can be defined by

$$G_{k|k}[h] = F_0[h] \cdot \frac{\sum_{\mathbf{y}\angle\mathbf{Z}_k} \prod_{\mathbf{W}\in\mathbf{y}} d_{\mathbf{W}}[h]}{\sum_{\mathbf{y}'\angle\mathbf{Z}_k} \prod_{\mathbf{W}\in\mathbf{y}'} d_{\mathbf{W}}[h]}, \tag{61}$$

where,

$$F_0[h] = exp(\mu s[(h-1)(1-p_D+p_D e^{-\lambda})]), \tag{62}$$

and where

$$d_{\mathbf{W}}[h] = \begin{cases} 1+\mu s[he^{-\gamma}p_D\iota_{\mathbf{z}}] & \text{if}\mathbf{W}=\{\mathbf{z}\} \\ \mu s[he^{-\gamma}p_D\prod_{\mathbf{z}\in\mathbf{W}}\iota_{\mathbf{z}}] & \text{if}|\mathbf{W}|\neq 1, \end{cases} \tag{63}$$

$$d_{\mathbf{W}} = d_{\mathbf{W}}[1] = \begin{cases} 1+\mu s[e^{-\gamma}p_D\iota_{\mathbf{z}}] & \text{if}\mathbf{W}=\{\mathbf{z}\} \\ \mu s[e^{-\gamma}p_D\prod_{\mathbf{z}\in\mathbf{W}}\iota_{\mathbf{z}}] & \text{if}|\mathbf{W}|\neq 1, \end{cases} \tag{64}$$

$$l_{\mathbf{z}}(\mathbf{x}) = \frac{\gamma(\mathbf{x})\cdot\phi_{\mathbf{z}}(\mathbf{x})}{\lambda c(\mathbf{z})}, \tag{65}$$

and

$$\mu = \int D_{k|k}(\mathbf{x})d\mathbf{x}. \tag{66}$$

Using the definition of the PHD in [2], the PHD $D_{k|k}[h]$ can be represented by

$$D_{k|k}[h] = \frac{\delta G_{k|k}[h]}{\delta\mathbf{x}}[1] \tag{67}$$

According to the product rule of the functional derivatives, we have

$$\begin{aligned}\frac{\delta G_{k|k}[h]}{\delta\mathbf{x}}[h] = \frac{\delta F_0}{\delta\mathbf{x}}[h]\cdot\frac{\sum_{\mathbf{y}\angle\mathbf{Z}_k}\prod_{\mathbf{W}\angle\mathbf{y}} d_{\mathbf{W}}[h]}{\sum_{\mathbf{y}'\angle\mathbf{Z}_k}\prod_{\mathbf{W}\angle\mathbf{y}'} d_{\mathbf{W}}[h]} \\ + F_0[h]\cdot\frac{\sum_{\mathbf{y}\angle\mathbf{Z}_k}\frac{\delta}{\delta\mathbf{x}}\prod_{\mathbf{W}\in\mathbf{y}} d_{\mathbf{W}}[h]}{\sum_{\mathbf{y}\angle\mathbf{Z}_k}\prod_{\mathbf{W}\in\mathbf{y}} d_{\mathbf{W}}[h]}\end{aligned} \tag{68}$$

The derivative of $F_0[h]$ in (62) can be calculated by

$$\frac{\delta F_0}{\delta\mathbf{x}}[h] = F_0[h]\cdot D_{k|k-1}\cdot(1-p_D(\mathbf{x})+p_D(\mathbf{x})e^{-\lambda(\mathbf{x})}) \tag{69}$$

Moreover,

$$\frac{\delta}{\delta\mathbf{x}}\prod_{\mathbf{W}\in\mathbf{y}} d_{\mathbf{W}}[h] = (\frac{\delta}{\delta\mathbf{x}}\prod_{\mathbf{W}\in\mathbf{y}} d'_{\mathbf{W}}[h])\cdot\sum_{\mathbf{W}\in\mathbf{y}}\frac{1}{d_{\mathbf{W}}[h]}\cdot\frac{\delta d_{\mathbf{W}}}{\delta}[h], \tag{70}$$

where

$$\begin{aligned}&\frac{\delta d_{\mathbf{W}}}{\delta\mathbf{x}}[h] \\ &= \begin{cases} D_{k|k-1}(\mathbf{x})\cdot e^{-\gamma(\mathbf{x})}\cdot p_D(\mathbf{x})\cdot\iota_{\mathbf{z}}(\mathbf{x}), & \mathbf{W}=\{\mathbf{z}\} \\ D_{k|k-1}(\mathbf{x})\cdot e^{-\gamma(\mathbf{x})}\cdot p_D(\mathbf{x})\cdot\prod_{\mathbf{z}\in\mathbf{W}}\iota_{\mathbf{z}}(\mathbf{x}), & |\mathbf{W}|\neq 1. \end{cases}\end{aligned} \tag{71}$$

Thus,

$$\frac{\delta d_{\mathbf{W}}}{\delta\mathbf{x}}[h] = D_{k|k-1}(\mathbf{x})\cdot e^{-\gamma(\mathbf{x})}\cdot p_D(\mathbf{x})\cdot\prod_{\mathbf{z}\in\mathbf{W}}\iota_{\mathbf{z}}(\mathbf{x}) \tag{72}$$

Then, substituting (69) and (72) into (68), we have

$$\begin{aligned}&\frac{1}{F[h]\cdot D_{k|k-1}(\mathbf{x})}\cdot\frac{\delta G_{k|k}[h]}{\delta\mathbf{x}}[h] \\ &= (1-p_D(\mathbf{x})+p_D(\mathbf{x})e^{-\gamma(\mathbf{x})})\cdot\frac{\sum_{\mathbf{y}\angle\mathbf{Z}_k}\prod_{\mathbf{W}\in\mathbf{y}} d_{\mathbf{W}}}{\sum_{\mathbf{y}'\angle\mathbf{Z}_k}\prod_{\mathbf{W}\in\mathbf{y}'} d_{\mathbf{W}}[h]} \\ &+ \sum_{\mathbf{y}\angle\mathbf{Z}_k}(\prod_{\mathbf{W}\in\mathbf{y}} d_{\mathbf{W}}[h])\cdot\frac{\sum_{\mathbf{W}\in\mathbf{y}}\frac{e^{-\gamma(\mathbf{x})}p_D(\mathbf{x})\prod_{\mathbf{z}\in\mathbf{W}}\iota_{\mathbf{z}}(\mathbf{x})}{d_{\mathbf{W}}[h]}}{\sum_{\mathbf{y}'\angle\mathbf{Z}_k}\prod_{\mathbf{W}\in\mathbf{y}'} d_{\mathbf{W}}}\end{aligned} \tag{73}$$

Setting $h = 1$, (73) yields to

$$\begin{aligned}
&\frac{D_{k|k}(\mathbf{x})}{D_{k|k-1}(\mathbf{x})} \\
&= 1 - p_D(\mathbf{x}) + p_D(\mathbf{x})e^{-\gamma(\mathbf{x})} + \sum_{\mathbf{y}\angle\mathbf{Z}_k}\left(\prod_{\mathbf{W}\in\mathbf{y}} d_{\mathbf{W}}\right) \\
&\quad \cdot \frac{\sum_{\mathbf{W}\in\mathbf{y}} \frac{e^{-\gamma(\mathbf{x})}p_D(\mathbf{x})\prod_{\mathbf{z}\in\mathbf{W}}\iota_{\mathbf{z}}(\mathbf{x})}{d_{\mathbf{W}}}}{\sum_{\mathbf{y}'\angle\mathbf{Z}_k}\prod_{\mathbf{W}\in\mathbf{y}'} d_{\mathbf{W}}} = 1 - p_D(\mathbf{x}) + p_D(\mathbf{x})e^{-\gamma(\mathbf{x})} \\
&\quad + \sum_{\mathbf{y}\angle\mathbf{Z}_k} \frac{\prod_{\mathbf{W}\in\mathbf{y}} d_{\mathbf{W}}}{\sum_{\mathbf{y}\angle\mathbf{Z}_k}\prod_{\mathbf{W}\in\mathbf{y}} d_{\mathbf{W}}} \cdot \sum_{\mathbf{W}\in\mathbf{y}} \frac{e^{-\gamma(\mathbf{x})}p_D(\mathbf{x})\prod_{\mathbf{z}\in\mathbf{W}}\iota_{\mathbf{z}}(\mathbf{x})}{d_{\mathbf{W}}}
\end{aligned} \tag{74}$$

To simplify (74), we define the coefficient

$$\omega_{\mathbf{y}} = \frac{\prod_{\mathbf{W}\in\mathbf{y}} d_{\mathbf{W}}}{\sum_{\mathbf{y}\angle\mathbf{Z}_k}\prod_{\mathbf{W}} d_{\mathbf{W}}}, \tag{75}$$

Using (75), (74) can be rewritten by

$$\begin{aligned}
\frac{D_{k|k}(\mathbf{x})}{D_{k|k-1}(\mathbf{x})} &= 1 - p_D(\mathbf{x}) + p_D(\mathbf{x})e^{-\gamma(\mathbf{x})} \\
&\quad + \sum_{\mathbf{y}\angle\mathbf{Z}_k} \omega_p \cdot \sum_{\mathbf{W}\in\mathbf{y}} \frac{e^{-\gamma(\mathbf{x})}p_D(\mathbf{x})\prod_{\mathbf{z}\in\mathbf{W}}\iota_{\mathbf{z}}(\mathbf{x})}{d_{\mathbf{W}}} \\
&= 1 - p_D(\mathbf{x}) + p_D(\mathbf{x})e^{-\gamma(\mathbf{x})} \\
&\quad + e^{-\gamma(\mathbf{x})}p_D(\mathbf{x}) \sum_{\mathbf{y}\angle\mathbf{Z}_k} \omega_p \cdot \sum_{\mathbf{W}\in\mathbf{y}} \frac{1}{d_{\mathbf{W}}} \cdot \prod_{\mathbf{z}\in\mathbf{W}} \iota_{\mathbf{z}}(\mathbf{x})
\end{aligned} \tag{76}$$

Finally, we can observe that (75) is the same as (7) in Section II-C.

REFERENCES

[1] R. Mahler, "PHD filters for nonstandard targets, I: Extended targets," in *Proc. 12th Int. Conf. Inf. Fusion*, Jul. 2009, pp. 915–921.

[2] R. P. S. Mahler, *Statistical Multisource-multitarget Information Fusion*, vol. 685. Boston, MA, USA: Artech House, 2007.

[3] G. W. Pulford, "Taxonomy of multiple target tracking methods," *IEE Proc.-Radar, Sonar Navigat.*, vol. 152, no. 5, pp. 291–304, Oct. 2005.

[4] S. S. Blackman, "Multiple hypothesis tracking for multiple target tracking," *IEEE Aerosp. Electron. Syst. Mag.*, vol. 19, no. 1, pp. 5–18, Jan. 2004.

[5] Y. Bar-Shalom and X. R. Li, *Multitarget-Multisensor Tracking: Principles and Techniques*. Storrs, CT, USA: YBS, 1995.

[6] M. Feldmann and D. Franken, "Tracking of extended objects and group targets using random matrices—A new approach," in *Proc. 11th Int. Conf. Inf. Fusion*, Jun./Jul. 2008, pp. 1–8.

[7] M. Feldmann, D. Fränken, and W. Koch, "Tracking of extended objects and group targets using random matrices," *IEEE Trans. Signal Process.*, vol. 59, no. 4, pp. 1409–1420, Apr. 2011.

[8] M. Xu, T. Li, Z. Wang, X. Deng, R. Yang, and Z. Guan, "Reducing complexity of HEVC: A deep learning approach," *IEEE Trans. Image Process.*, vol. 27, no. 10, pp. 5044–5059, Oct. 2018.

[9] G. Vivone, K. Granström, P. Braca, and P. Willett, "Multiple sensor measurement updates for the extended target tracking random matrix model," *IEEE Trans. Aerosp. Electron. Syst.*, vol. 53, no. 5, pp. 2544–2558, Oct. 2017.

[10] C. Magnant, S. Kemkemian, and L. Zimmer, "Joint tracking and classification for extended targets in maritime surveillance," in *Proc. IEEE Radar Conf. (RadarCon)*, Apr. 2018, pp. 1117–1122.

[11] J. Lan and X. R. Li, "Tracking of maneuvering non-ellipsoidal extended object or target group using random matrix," *IEEE Trans. Signal Process.*, vol. 62, no. 9, pp. 2450–2463, May 2014.

[12] M. Beard, S. Reuter, K. Granström, B.-T. Vo, B.-N. Vo, and A. Scheel, "A generalised labelled multi-Bernoulli filter for extended multi-target tracking," in *Proc. 18th Int. Conf. Inf. Fusion*, Jul. 2015, pp. 991–998.

[13] M. Beard, B. T. Vo, and B. N. Vo, "Bayesian multi-target tracking with merged measurements using labelled random finite sets," *IEEE Trans. Signal Process.*, vol. 63, no. 6, pp. 1433–1447, Mar. 2015.

[14] M. Beard, S. Reuter, K. Granström, B.-T. Vo, B.-N. Vo, and A. Scheel, "Multiple extended target tracking with labeled random finite sets," *IEEE Trans. Signal Process.*, vol. 64, no. 7, pp. 1638–1653, Apr. 2016.

[15] R. Mahler, "Engineering statistics for multi-object tracking," in *Proc. IEEE Workshop Multi-Object Tracking*, Jul. 2005, pp. 53–60.

[16] K. Gilholm, S. Godsill, S. Maskell, and D. Salmond, "Poisson models for extended target and group tracking," *Proc. SPIE*, vol. 5913, pp. 59130R1–59130R12, Sep. 2005.

[17] Z. Liu, Z. Wang, M. Xu, L. Yang, and J. Liu, "A novel CIF-based SMC-PHD approach for tracking multiple nonlinear targets," in *Proc. IEEE Radar Conf. (RadarCon)*, May 2015, pp. 555–560.

[18] Z. Liu, Z. Wang, and M. Xu, "Cubature information SMC-PHD for multi-target tracking," *Sensors*, vol. 16, no. 5, p. 653, 2016.

[19] Y. Zhang and H. Ji, "A robust and fast partitioning algorithm for extended target tracking using a Gaussian inverse Wishart PHD filter," *Knowl. Based Syst.*, vol. 95, no. 1, pp. 125–141, Mar. 2016.

[20] S. Li, M. Xu, Z. Wang, and X. Sun, "Optimal bit allocation for CTU level rate control in HEVC," *IEEE Trans. Circuits Syst. Video Technol.*, vol. 27, no. 11, pp. 2409–2424, Nov. 2017.

[21] K. Granström, C. Lundquist, and U. Orguner, "A Gaussian mixture PHD filter for extended target tracking," in *Proc. 13th Int. Conf. Inf. Fusion*, Jul. 2010, pp. 1–8.

[22] K. Granström, U. Orguner, R. Mahler, and C. Lundquist, "Corrections on: 'Extended target tracking using a Gaussian-mixture PHD filter,'" *IEEE Trans. Aerosp. Electron. Syst.*, vol. 53, no. 2, pp. 1055–1058, Apr. 2017.

[23] M. Xu, Y. Song, J. Wang, M. Qiao, L. Huo, and Z. Wang, "Predicting head movement in panoramic video: A deep reinforcement learning approach," *IEEE Trans. Pattern Anal. Mach. Intell.*, to be published.

[24] K. Granström, C. Lundquist, and U. Orguner, "Extended target tracking using a Gaussian-mixture PHD filter," *IEEE Trans. Aerosp. Electron. Syst.*, vol. 48, no. 4, pp. 3268–3286, Oct. 2012.

[25] J. Chen, N. Wang, L. Ma, and B. Xu, "Extended target probability hypothesis density filter based on cubature Kalman filter," *IET Radar, Sonar Navigat.*, vol. 9, no. 3, pp. 324–332, 2015.

[26] J. Yang, P. Li, L. Yang, and H. Ge, "An improved ET-GM-PHD filter for multiple closely-spaced extended target tracking," *Int. J. Control, Automat. Syst.*, vol. 15, no. 1, pp. 468–472, 2017.

[27] Y. Zhang and H. Ji, "A novel fast partitioning algorithm for extended target tracking using a Gaussian mixture PHD filter," *Signal Process.*, vol. 93, no. 11, pp. 2975–2985, 2013.

[28] X. Shen, Z. Song, H. Fan, and Q. Fu, "RFS-based extended target multipath tracking algorithm," *IET Radar, Sonar Navigat.*, vol. 11, no. 7, pp. 1031–1040, Jul. 2017.

[29] B. Ristic, D. Clark, B.-N. Vo, and B.-T. Vo, "Adaptive target birth intensity for PHD and CPHD filters," *IEEE Trans. Aerosp. Electron. Syst.*, vol. 48, no. 2, pp. 1656–1668, Apr. 2012.

[30] Y. Zhu, S. Zhou, H. Zou, and K. Ji, "Probability hypothesis density filter with adaptive estimation of target birth intensity," *IEE Radar, Sonar Navigat.*, vol. 10, no. 5, pp. 901–911, Jun. 2016.

[31] X. Zhou, Y. F. Li, and B. He, "Entropy distribution and coverage rate-based birth intensity estimation in GM-PHD filter for multi-target visual tracking," *Signal Process.*, vol. 94, pp. 650–660, Jan. 2014.

[32] J. Wu, K. Li, Q. Zhang, W. An, Y. Jiang, X. Ping, and P. Chen, "Iterative RANSAC based adaptive birth intensity estimation in GM-PHD filter for multi-target tracking," *Signal Process.*, vol. 131, pp. 412–421, Feb. 2017.

[33] C. Peng and W. Ye, "An improved adaptive ET-PHD algorithm for newborn target intensity," in *Proc. IEEE 3rd Adv. Inf. Technol., Electron. Automat. Control Conf. (IAEAC)*, Oct. 2018, pp. 2137–2142.

[34] K. P. B. Chandra, D.-W. Gu, and I. Postlethwaite, "Square root cubature information filter," *IEEE Sensors J.*, vol. 13, no. 2, pp. 750–758, Feb. 2013.

[35] R. Mahler, "'Statistics 102' for multisource-multitarget detection and tracking," *IEEE J. Sel. Topics Signal Process.*, vol. 7, no. 3, pp. 376–389, Jun. 2013.

[36] T. Bailey, B. Upcroft, and H. Durrant-Whyte, "Validation gating for non-linear non-Gaussian target tracking," in *Proc. 9th Int. Conf. Inf. Fusion*, Jul. 2007, pp. 1–6.

[37] S. Reuter, B.-T. Vo, B.-N. Vo, and K. Dietmayer, "The labeled multi-Bernoulli filter," *IEEE Trans. Signal Process.*, vol. 62, no. 12, pp. 3246–3260, Jun. 2014.
[38] I. Arasaratnam and S. Haykin, "Cubature Kalman filters," *IEEE Trans. Autom. Control*, vol. 54, no. 6, pp. 1254–1269, Jun. 2009.
[39] B. N. Vo and W. K. Ma, "The Gaussian mixture probability hypothesis density filter," *IEEE Trans. Signal Process.*, vol. 54, no. 11, pp. 4091–4104, Nov. 2006.
[40] M. Longbin, S. Xiaoquan, Z. Yiyu, S. Z. Kang, and Y. Bar-Shalom, "Unbiased converted measurements for tracking," *IEEE Trans. Aerosp. Electron. Syst.*, vol. 34, no. 3, pp. 1023–1027, Jul. 1998.
[41] D. Schuhmacher, B.-T. Vo, and B.-N. Vo, "A consistent metric for performance evaluation of multi-object filters," *IEEE Trans. Signal Process.*, vol. 56, no. 8, pp. 3447–3457, Aug. 2008.
[42] H. Zhang, Z. Jing, and S. Hu, "Gaussian mixture CPHD filter with gating technique," *Signal Process.*, vol. 89, no. 8, pp. 1521–1530, 2009.

ZHE LIU received the B.E. degree from the North China Institute of Technology, in 2003, the M.S. degree from the North University of China, in 2006, and the Ph.D. degree from Beihang University, in 2017. He is currently a Lecturer with the North University of China. His research interests include signal processing, target tracking, and radar countermeasure.

LINNA JI received the B.S. degree from the North University of China, in 2010, and the Ph.D. degree in signal and information processing from the North University of China, in 2015. Her current research interest includes infrared multi-source image fusion.

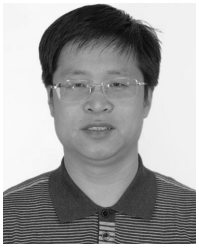

FENGBAO YANG received the Ph.D. degree in measurement technology and instrument from the North University of China, Taiyuan, China, in 2003. From 2004 to 2007, he was a Postdoctoral Research Fellow with the Beijing Institute of Technology. He is currently a Full Professor with the North University of China. His current research interests include information fusion, performance detection and evaluation of complex systems, and information fusion theory of uncertainty. He presided more than two items of the National Natural Science Foundation.

XIQIANG QU received the B.E. degree from the North China Institute of Technology, in 1997, the M.S. degree from the North University of China, in 2006, and the Ph.D. degree from the Beijing Institute of Technology, in 2011. He is currently with the North University of China as a Lecturer. His research interest includes target tracking.

ZHILIANG YANG received the B.E. degree from the North China Institute of Technology, in 2003, the M.S. degree from the North University of China, in 2007, and the Ph.D. degree from the Beijing Institute of Technology, in 2015. He is currently a Lecturer with the North University of China. His research interests include wireless channel modelling, physical layer security, and channel coding.

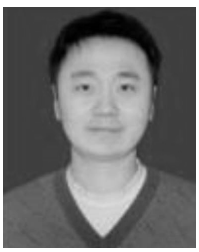

DONGZE QIN received the B.E. degree from the North China Institute of Technology, in 2003, the M.S. degree from the North University of China, in 2006, and the Ph.D. degree from the Beijing Institute of Technology, in 2013. Since June 2014, he has been with the North University of China as an Associate Professor. His research interest includes laser fusing.